Helium in silicon: Thermal-desorption investigation of bubble precursors

F. Corni, C. Nobili, G. Ottaviani, R. Tonini, and G. Calzolari
Istituto Nazionale per la Fisica della Materia (I.N.F.M.) and Dipartimento di Fisica, University of Modena, I-41100 Modena, Italy

G. F. Cerofolini and G. Queirolo
SGS Thomson, I-20041 Agrate Brianza, Milano, Italy

(Received 21 October 1996; revised manuscript received 7 April 1997)

Thermal desorption measurements are performed on (100)-oriented p-type Si wafers implanted with He ions at 20 keV. The doses have been selected in order to produce crystal damage avoiding the formation of detectable bubbles. The He effusion kinetics, studied both in isothermal and in constant heating rate conditions, exhibit effective activation energy heterogeneity indicating the presence of various kinds of traps, precursor of the bubbles. The energy distribution results peaked at about 1.1 eV with an exponential decay towards higher energies and a width of about 0.2 eV. A semiquantitative model, based on the present knowledge about the Si:He system, is proposed, that accounts for He filled nanoblisters formation through interstitial He clustering and precipitation. The observed energy heterogeneity is ascribed to variations of the He solution energy from these cavities due to He-He and He-wall interactions. [S0163-1829(97)05035-2]

I. INTRODUCTION

Room-temperature He implantation into silicon at high doses (of the order of 10^{16} cm^{-2}) produces cavities of various sizes filled with He. The subsequent thermal treatments, at temperatures above 700 °C, cause He to effuse and the remaining voids to coalesce producing empty bubbles with dimensions in the range 5–100 nm.[1–4] The walls of these cavities, supposedly perfectly clean, are of great scientific interest either for fundamental[5–8] or for applied research.[3,4,9–12] Bubbles are observed in silicon whenever a critical He concentration of 3.5×10^{20} cm^{-3} is exceeded, independent of the energy used during room-temperature implantation.[3,4] Though many papers have been devoted to the search for the conditions of preparing the bubbles with convenient dimensions and located at the desired depths, the microscopic interactions at the origin of the formation of the bubbles are not adequately investigated yet, in particular, very little is known about the physical phenomena that produce the release of He atoms and create the nanocavities precursors of the bubbles.

Bubbles in ion-implanted materials are the end products of several processes which include the interactions of He with the defects, the creation of nanocavities, the release of He atoms, and finally, the agglomeration of nanocavities. The defect production is well described by simulation codes based on Monte Carlo or molecular-dynamic approaches that simulate ion-matter interactions. Although He in metals has been extensively investigated, very few thermodynamic and kinetic data are available on the Si:He system. The solution energy, $\Delta H_s \approx 0.9$ eV, of He in Si can be evaluated as the difference between the permeation enthalpy of 1.74 eV (Ref. 13) and the migration energy E_m of 0.8 eV.[14] Calculations of heats of solution of the He atom in various Si interstitial sites performed by Alatalo, Puska, and Nieminen[15] adopting a Car-Parrinello first-principle molecular-dynamics scheme give the absolute minimum value of 0.88 eV in very good agreement with the experiment. This value is found for He in the tetrahedral site T_d. In the same work the migration energy is ascribed to the energy barrier encountered during the zigzag movement from the tetrahedral to the hexagonal sites; the value estimated is 0.84 eV, in agreement with the experiment. It is also evidenced that the single vacancy does not act as a trapping center for He atoms because of its high electronic density compared to that in interstitial regions. The same authors show that two He atoms in a perfect crystal tend to occupy adjacent T_d interstitial sites so minimizing the total energy due to lattice relaxation. The energy gain compared to the case of two single interstitial He atoms is 0.08 eV, which can be regarded as binding energy of the He atom pair in Si. The He pairs are therefore stable at room temperature and the process of pairing can lead to clustering. The activation energy for He release from stable bubbles[1] produced by high doses of ion implantation is $E_{\text{bubble}}=1.7$ eV. In permeation experiments,[13] where similar results have been obtained, the activation energy has two contributions: one from the enthalpy of solution of He and the other from the migration energy. The same contributions should be present in the ion implantation cases and E_{bubble} should be regarded as the upper limit of the dissociation energy of He from any defect in Si, if the van der Waals binding can be neglected.

The purpose of this work is the study of the defects, precursors of the bubbles in Si, by means of their interaction with He employing thermal-desorption (TD) spectrometry. The experiment is performed in an unusual fashion since He is used both for damage production and as a probe for defects. In addition, for the energy and doses used, the defect density and He concentration around the projected range of the implantation profile can reach values such that the phenomena of retrapping as well as multiple decoration of the traps can appreciably affect the desorption process. In these conditions, the interpretation of the TD spectra must take into account possible heterogeneity in the trap binding energy produced by the different sizes of traps and by their effect on diffusion. For the interpretation of the experimental

results, a semiquantitative model will be proposed in the discussion accounting for the formation of small vacancy cluster precursors of the bubbles.

II. THERMAL-DESORPTION SPECTROMETRY

Thermal-desorption spectrometry, originally developed for surface analysis,[16,17] is also a powerful instrument for studying defects in bulk by means of their interactions with noble gases, e.g., He. The He atoms, brought into the material by implantation, tend to occupy regions of minimum electron density where they are trapped. He implantation close to the critical doses for bubble formation produces damage mainly composed of point defects and small defect clusters. It is reasonable to expect that the He atoms result, trapped by a population of sinks, characterized by a slight dispersed activation energy for He dissociation. In this section, we first recall the fundamental equations of the homogeneous He emission, then we will derive the equation for the case of energy heterogeneity of the traps by analogy with the case of chemisorption and adsorption on real surfaces.[18,19]

A TD measurement is performed by recording the considered gas partial pressure, proportional to the desorption rate $r(t)=|dC/dt|$ (the amount of He leaving the unit surface per unit time), during sample heating in a known temperature-time profile, usually constant in isothermal measurements, or with constant slope in constant ramp rate (CRR) measurements.

In the presence of singly occupied noninteracting traps of only one kind, the desorption consists of He release with first-order kinetics described by the differential equation:

$$\frac{dC}{dt}=-\frac{C}{\tau(T,E)}, \tag{1}$$

where $\tau(T,E)=\tau_0\exp(E/k_BT)$ is a characteristic time, thermally activated, function of the absolute temperature T and of the binding energy E proper of the trap; k_B is the Boltzmann constant.

Denoting by C_0 the total amount of matter involved in the process, the isothermal solution, with initial condition $C(0)=C_0$, is given by

$$C(t)=C_0\exp\left(-\frac{t}{\tau(T,E)}\right). \tag{2}$$

The desorption rate resulting from the measurement is given by

$$r(t)=-\frac{dC}{dt}=\frac{C_0}{\tau}\exp\left(-\frac{t}{\tau}\right). \tag{3}$$

The energy heterogeneity can be introduced through the definition of the activation energy distribution $\varphi(E)$, where $\varphi(E)dE$ represents the fraction of material that desorbs with activation energy between E and $E+dE$. The normalization condition requires that $\int_0^{+\infty}\varphi(E)dE=1$. The heterogeneous isotherm $C_h(t)$ is then constructed by observing that all homogeneous isotherms $C(t,E)$ at time t contribute to the desorption process, each weighted by its own probability:

$$C_h(t)=\int_0^{+\infty}C(t,E)\varphi(E)dE. \tag{4}$$

This approach does not distinguish the case of a distribution of populations of traps simultaneously present and stable (fixed heterogeneity) from the very different case in which the process at time t is characterized by a single activation energy $E(C)$ function of $C(t)$ (induced heterogeneity).

According to Eq. (2), we use the family of functions

$$C(t,E)=C_0\exp\left(-\frac{t}{\tau_0\exp(E/k_BT)}\right), \tag{5}$$

as a kernel of Eq. (4). As a distribution function we assume

$$\varphi(E)=\begin{cases}0, & 0\leqslant E<E_{\min}\\ A\ \exp(-E/\Delta), & E_{\min}\leqslant E\leqslant E_{\max}\\ 0, & E>E_{\max},\end{cases} \tag{6}$$

where A is a normalization constant, Δ a fitting parameter that measures the energy spread, and $E_{\min}$ and $E_{\max}$ are the extremes of the activation energies that appreciably contribute to the desorption process. Equation (6) is widely used in literature and the combinations of the values of the three parameters Δ, $E_{\min}$, and $E_{\max}$ allow a wide class of possible situations to be described: (a) boxlike distribution (producing a pure time-logarithm law) for $E_{\max}-E_{\min}\ll\Delta$ and $\Delta\gg k_BT$; (b) exponential distribution, for $E_{\max}\gg E_{\min}+\Delta$, Δ finite and greater than k_BT; and (c) energy homogeneity for $\Delta<k_BT$. The case of energy distribution monotonically increasing is not considered since it is not compatible with the experimental results, as will be shown later.

In the fitting procedure, a crucial point is the choice of the preexponential factor τ_0 in Eq. (5) since it determines the absolute values of activation energies. What is strictly necessary is a guess of its order of magnitude that can be evaluated performing the fits using the parameter τ instead of E [by the substitution $E\rightarrow k_BT\ \ln(\tau/\tau_0)$] and from an Arrhenius plot of $\tau_{\min}$.

The function of the isothermal rate is given by (see the appendix)

$$r_h(t)\propto B\ \frac{d}{dt}\left[t^{-k_BT/\Delta}\Gamma\left(\frac{k_BT}{\Delta},\frac{t}{\tau_{\min}},\frac{t}{\tau_{\max}}\right)\right], \tag{7}$$

where B is a constant, $\tau_{\min}=\tau_0\exp(E_{\min}/k_BT)$, $\tau_{\max}=\tau_0\exp(E_{\max}/k_BT)$, and $\Gamma(s,a,b)=\int_a^b x^{s-1}\exp(-x)dx$ is the generalized incomplete gamma function.

In Fig. 1 we report calculated heterogeneous $r_h(t)$ for the three mentioned cases. In the same figure we have overlaid the same numerical data referred to convenient ordinate scales on the right axes to furnish a rule for the recognition of the three kinds of heterogeneity. Cases (a) and (c) are identified by a straight-line behavior of the $1/r_h(t)$ and $\ln[r_h(t)]$ plots respectively, while case (b) can be recognized by a slight superlinear deviation in the $1/r_h(t)$ plot, accentuating with decreasing Δ.

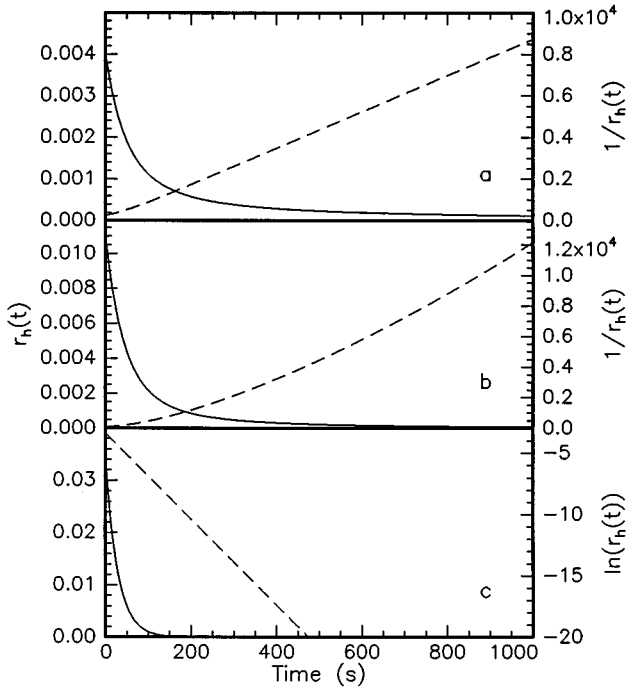

FIG. 1. Calculated isothermal desorption rates for three different energy heterogeneity conditions assuming $\tau_0 = 10^{-10}$ s. (a) Boxlike energy distribution ($E_{min} = 1.2$ eV, $E_{max} = 2$ eV, $\Delta = 10$ eV); (b) exponential distribution ($E_{min} = 1.2$ eV, $E_{max} = 2$ eV, $\Delta = 0.1$ eV); (c) homogeneity [Eq. (3) with $E = 1.2$ eV]. Solid lines are referred to the left axes, dashed lines are referred to the right axes.

III. EXPERIMENT AND RESULTS

It is believed that no voids or bubbles are observed in silicon after annealing if they were not already present in the as-implanted sample.[4] This means that the implantation conditions are the main parameters for bubble production. We have chosen an implantation energy of 20 keV in order to drive the ions deep into the samples and avoid He effusion during implantation or during the storage at room temperature. The implantation profile was simulated by means of the TRIM95 code[20] in order to estimate the influences suitable for the experiment. At 20 keV the He projected range R_p is expected to be about 235 nm with a straggling ΔR_p of 85 nm, hence an implantation of some 10^{15} cm^{-2} is expected to produce a maximum He concentration slightly below the critical concentration for bubble formation.

Four 150−mm, p-type (1.7–2.5 Ω cm), Czochralski-grown, (100)-oriented silicon wafers were implanted at 20 keV and influences 1.4×10^{15}, 5×10^{15}, 2×10^{16}, and 3.5×10^{16} cm^{-2}, respectively, with a beam current of about 8 μA cm^{-2} and keeping the sample holder near room temperature. Sample tilt was 7° to avoid ion channeling.

TD measurements were performed in a vacuum chamber of volume 2000 cm^3 where the sample is in contact with a heater made by a rigid stainless-steel bar. Silver paint is used to ensure good thermal contacts both for the sample and for a Chromel-Alumel thermocouple, placed on the back side of the bar, just behind the sample. The chamber is equipped with a turbomolecular pump (with pumping speed for He of 370 l s^{-1}) that mounts on the exhaust of a second turbomolecular pump that, by means of the counterflow method, directs preferentially the He atoms towards the head of a quadrupole. The counter-flow method is based on the principle of mass-dependent compression: the second turbomolecular pump (pumping speed for air of 50 l s^{-1}, for He of 2 l s^{-1}) functions as a mass separator allowing light gases to pass through to the mass spectrometer against the direction of the evacuation flux. The first pump guarantees a prompt He evacuation from the sample chamber, while the particular position of the quadrupole, along the only path permitted to the gas, allows a direct evaluation with high sensitivity of the actual He flux leaving the sample. The response time to a He excitation is below 1 s, the exhaustion time is below 4 s, and the minimum detectable flux is 5×10^{-10} mbar l s^{-1}. Both isothermal and CRR desorption measurements were performed. All the thermal treatments started from a temperature of 50 °C; for isothermal measurements the desired annealing temperature was reached with a ramp of 60 °C min^{-1}, while for CRR measurements the maximum achieved temperature was 800 °C.

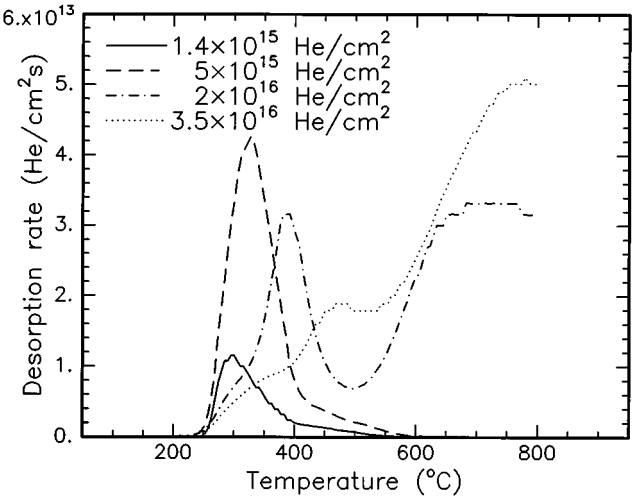

FIG. 2. TD spectra (heating rate 45 °C min^{-1}) of room-temperature He-implanted silicon of 20 keV at different doses.

Figure 2 reports the He CRR desorption spectra (heating rate 45 °C min^{-1}) of the four samples. In all the cases the He release starts at 250 °C with a maximum desorption rate in the range 250–500 °C: the higher the dose, the higher the temperature. The samples with the two highest doses present a second large broad peak at about 700 °C that, for shape and temperature position, could be due to He released from bubbles.[1,21] Transmission electron microscope images in cross-sectional conditions moreover confirm the presence of the bubbles only in the samples that have the peak at 700 °C. For the aim of this work was selected the 5×10^{15} cm^{-2} sample since it does not contain bubbles, at least for the sensitivity of our TD system and for the electron microscope resolution. In the following, we will refer to this sample, if not otherwise stated. CRR measurements, in addition to that shown in Fig. 2, was performed at 4 °C min^{-1} and 400 °C min^{-1}; even for the fastest ramp the pumping system was able to adequately exhaust the sample chamber. The desorption spectra at the three different heating rates are shown in Fig. 3. As expected, for a kinetically controlled process, the peaks shift towards higher temperatures as the

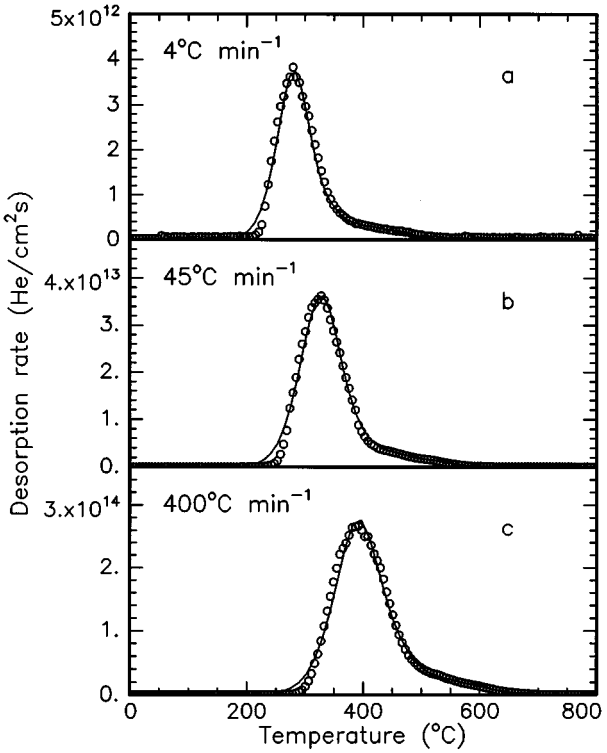

FIG. 3. CRR spectra of the 5×10^{15} cm^{-2} sample at different heating rates: (a) 4 °C min^{-1}, (b) 45 °C min^{-1}, (c) 400 °C min^{-1} (circles). The solid lines are calculated in the hypothesis of an energy distribution as shown in Fig. 8.

ramp rate is increased. The maxima are positioned at 285, 330, and 390 °C, respectively.

The isothermal treatments were performed at 190, 200, 250, 270, and 300 °C. These temperatures have been selected compatibly with the characteristics of the measurement system: the minimum temperature, 190 °C, ensures desorption rates significantly higher than the instrumental sensitivity and the maximum temperature, 300 °C, is the highest controlled temperature without appreciable He loss before temperature stabilization. The He desorption rate at 250 °C as a function of time is reported in Fig. 4; it reaches a maximum at about 190 s, then decreases monotonically with time. After 250 min some He is still retained in the sample. In the inset it is shown that the spectrum (solid line) obtained in the same sample cooled at room temperature and then heated at 45 °C min^{-1}. As a comparison, it is reported the spectrum (dashed line) was obtained in the same CRR conditions but from a sample not previously heat treated. The two curves are practically superimposed in the 400–600 °C temperature range.

In order to check if the time to reach the maximum He effusion rate is a physical phenomenon connected to the sample or is an instrumental artifact (due, for example, to conductance or sample thermalization delay times), an isothermal measurement at 250 °C was interrupted when the He flux was at the maximum and restarted after the sample was left for few minutes at room temperature. Figure 5 compares the measured rates during the first seconds of the isothermal treatments before and after the interruption. In the curve referred to in the second run, the spike around $t=0$ is due to temperature fluctuations during the heater stabilization at the

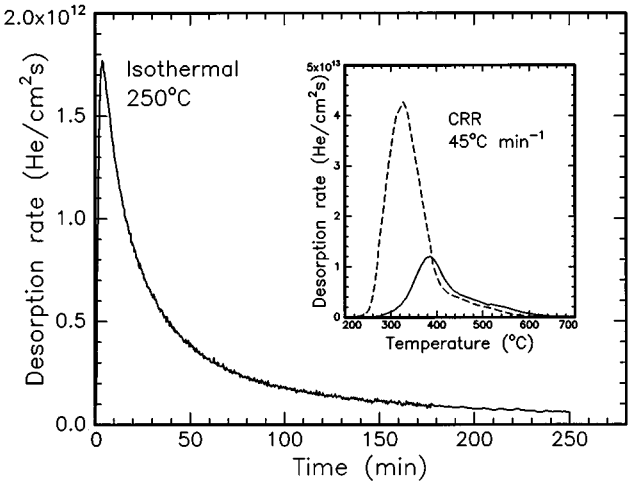

FIG. 4. Desorption rate at 250 °C as a function of time. The inset reports the subsequent CRR spectrum at 45 °C min^{-1} (solid line) compared to the reference spectrum of the as-implanted sample (dashed line).

end of the initial 60 °C min^{-1} ramp. The maximum temperature experienced by the sample is 253 °C for 5 s. The two curves are one being the continuation of the other provided that the second one is shifted by about 200 s afterwards; the result of their union reproduces, considering an experimental error in temperature reproducibility of ±2 °C, the 250 °C noninterrupted isothermal measurement of Fig. 4. This indicates that the experimental conditions do not modify the status of aggregation of He and, moreover, that the rising part

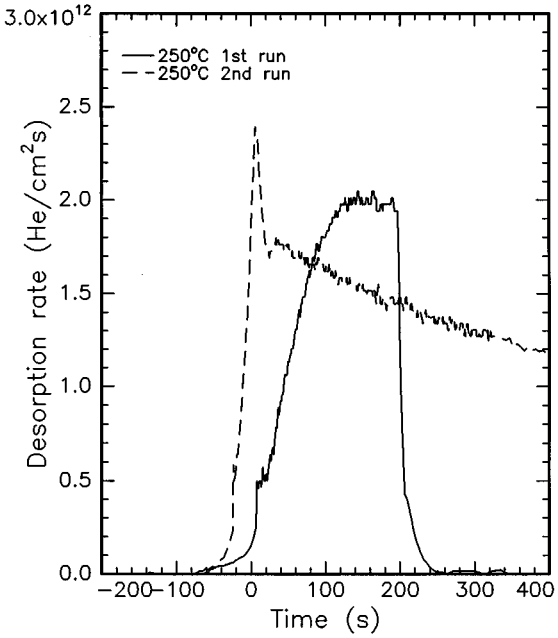

FIG. 5. Desorption rate during two subsequent isothermal treatments at 250 °C on the same sample. The first anneal (solid line) proceeded until the He flux reached the maximum value, then the sample was cooled down to room temperature (at about $t=200$ s). After 10 min, the second isothermal treatment was started and completed. The time axes are so aligned as $t=0$ corresponds in both cases to the time when the sample temperature reached 250 °C.

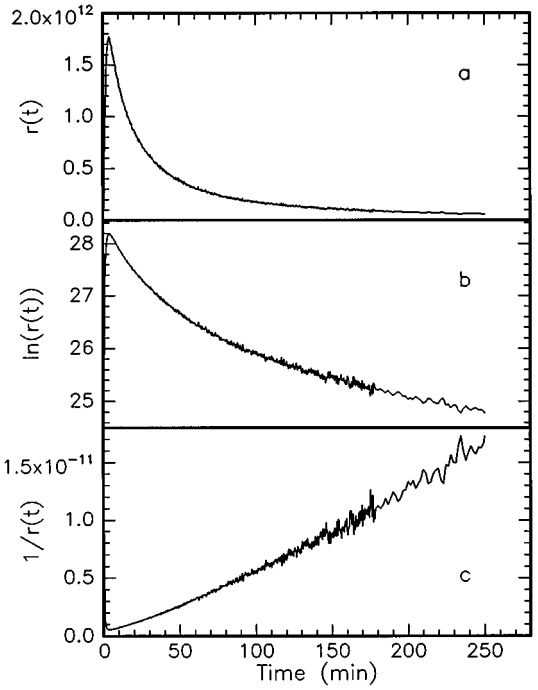

FIG. 6. Isothermal He desorption rate at 250 °C as a function of time in (a) linear scale, (b) logarithmic scale, and (c) inverse scale.

and the decreasing part of $r(t)$ can be ascribed to two sequential phenomena.

IV. DATA ANALYSIS

Thermal desorption measurements, especially in CRR conditions, cannot be univocally interpreted since the same results can be obtained by suitable combinations of various processes with different kinetics. As a consequence, before analyzing the data in detail, it is necessary to identify the kind of kinetics involved in He release.

A. Preliminary observations

The isothermal measurements present first of all a rise time t_r, here defined as the time required for the He to reach the highest desorption rate, monotonically decreasing with temperature. The rise time cannot be due to conventional diffusion time, τ_{diff}, of He from the implantation peak. In fact, using literature data[14] for the diffusion coefficient D, at 250 °C, $\tau_{\text{diff}}=R_p^2/D\approx 4$ s while $t_r=190$ s, about two orders of magnitude higher.

To investigate the kind of kinetics of the subsequent decreasing part of $r(t)$, in Fig. 6 are reported the experimental data obtained at 250 °C and plotted in various ways, (a) as $r(t)$, (b) as $\ln[r(t)]$, (c) as $1/r(t)$. Higher integer negative powers of the rate are ignored when corresponding to kinetics orders greater than one. No linear dependence is observed in the logarithmic plot [Fig. 6(b)] excluding pure first-order kinetics, while a slight superlinear dependence is obtained in Fig. 6(c). Such behavior, according to the scheme of Sec. II, evidences the presence of energy heterogeneity, with an energy spread $\Delta > k_B T$. Energy heterogeneity means, in this case, that the He effusion can be thought of as the superimposition of different contributions with kinetics of as many, little-differing, activation energies. Evidence of the soundness of the hypothesis of energy heterogeneity can be deduced also from this inset of Fig. 4: after an isothermal treatment at 250 °C, the He remaining in the sample desorbs in a narrower temperature range and shifted towards higher temperatures compared to the case of the as-implanted sample, suggesting the presence of a fraction of He atoms released from traps to which it is bonded more strongly. Also in this case, the characteristic time for conventional diffusion τ_{diff} results in two orders of magnitude lower than the characteristic time τ_m of the isothermal measurement estimated as the absolute minimum of the function $|r(t)/C(t)|$. For example, at 250 °C, τ_m is about 200 s which should be compared with the previously calculated $\tau_{\text{diff}}\approx 4$ s.

Analyzing the CRR measurements and focusing the attention, for example, on the 45 °C min^{-1} spectrum of Fig. 3(b), it is clear that the desorption peak presents an inappropriate shape for pure first-order kinetics, asymmetric towards the high temperatures with a long tail from about 400 up to 600 °C. An objective indication can be obtained by means of the skewness parameters χ_f defined by Chan, Aris, and Weinberg,[22] calculated at various fractions f of the maximum. All the skewness parameters are inconsistent with the theoretical predicted values for homogeneous first-order kinetics; in the case of half maximum, the experimental value of $\chi_{1/2}$ is $+5$ versus a predicted theoretical value of -15.

The previous qualitative phenomenological observations allow us to conclude that we are in the presence of a desorption process that requires a finite time to reach the maximum efficiency, then decreases and vanishes in a long time, with a character of energy heterogeneity leading to strong deviations from the pure homogeneous first-order kinetics. The diffusion of He in a defect-free region is not the limiting process.

B. Isothermal measurements

The data shown in Fig. 5 indicate that the rising part and the decreasing part of the desorption rate are due to two separate, sequential processes, and in this way they will be treated. Figure 7 shows an Arrhenius plot of t_r. No point at 300 °C has been reported because the maximum desorption rate was reached during thermalization. The rise time results are thermally activated, with an effective activation energy $E_r=(1.30\pm 0.05)$ eV.

The analysis of the decreasing part requires a fitting procedure of the experimental data using a parametric heterogeneous isotherm. At present, we are not able to select on a physical basis a suitable distribution function and we assume the widely employed expression for $\varphi(E)$ given by Eq. (6). Table I reports the values of the fitting parameters of Eq. (7) for the five employed temperatures. The relative uncertainty on τ_{min} is about 5% while on Δ is about 30%. The major sensitivity and precision is on the parameter τ_{min} which is the dominant contribution in the effusion kinetics, while τ_{max} can be evaluated only as a lower limit since the fast decreasing character of the assumed distribution function makes it ineffective above a certain value. The Arrhenius plot of τ_{min} furnishes the corresponding effective activation energy, the minimum of the distribution E_{min}, as well as the preexponential factor τ_0 that can be adopted as a guess of the pref-

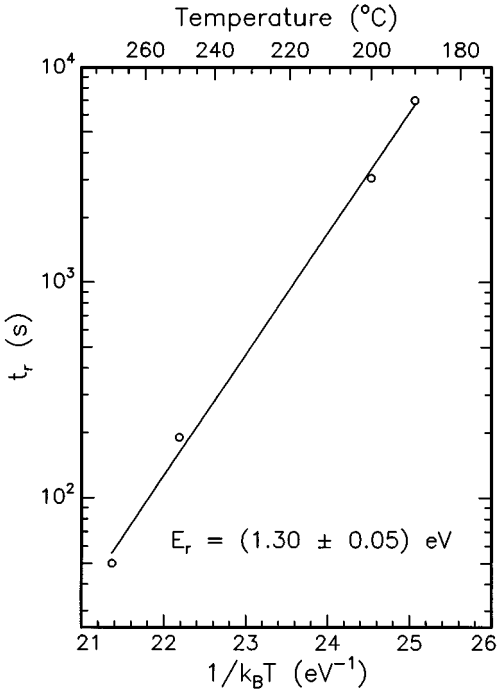

FIG. 7. Arrhenius plot of the rise time t_r in the isothermal measurements.

actor for the whole distribution. The values are $E_{\min}=(1.17 \pm 0.08)$ eV and 6×10^{-10} s$<\tau_0<3\times10^{-8}$ s. Figure 8 reports the effective activation energy distribution $\varphi(E)$ is representative of the five isothermal measurements, assuming $\tau_0=4\times10^{-9}$ s. The boundaries of variation of $\varphi(E)$ are marked considering the uncertainty on Δ. The value of $E_{\max}$ is not indicated for the indetermination on $\tau_{\max}$; however, the curve has been cut at 1.7 eV, considered the maximum value of dissociation energy of He from any defect in Si.

C. CRR measurements

According to the previous analysis of the isothermal measurements the experimental peak in CRR conditions can be thought of as composed of several close peaks, with activation energies above 1.1 eV. To introduce the energy heterogeneity in the theoretical peak construction we adopt the description in terms of energy distribution function and perform a best fit approximation of the $\varphi(E)$ segmented into adjacent steps of constant height, assuming the previously estimated preexponential factor. The fitting curves are superimposed on the experimental ones in Fig. 3. They match fairly well in the entire spectrum. The slight anomalies observed when effusion starts to occur can be interpreted as a consequence of the non-negligible time required for He to be emitted from the sample surface, also reflected by the presence of the rise time in the isothermal measurements. The resulting effective energy distribution is reported in Fig. 8 as histogram. The error bars are the ranges of variation of the fitted values for the three employed sample heating rates.

TABLE I. Values of the parameters obtained by fitting the isothermal TD measurements on the 5×10^{15} cm^{-2} sample with Eq. (7).

Temperature (°C)	$\tau_{\min}$ (s)	$\tau_{\max}$ (s)	Δ (eV)
190	17 500	$\geqslant3\times10^7$	0.1
200	6000	$\geqslant1\times10^6$	0.15
250	800	$\geqslant2\times10^5$	0.2
270	180	$\geqslant2\times10^5$	0.2
300	50	$\geqslant1\times10^5$	0.2

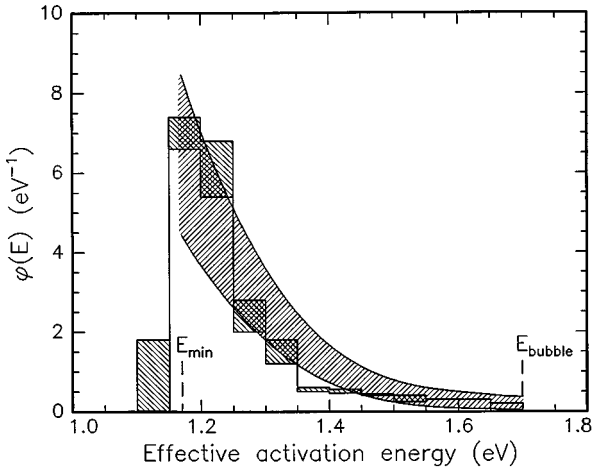

FIG. 8. Distribution functions of the effective activation energies for the release of He obtained from the isothermal (curve) and the CRR (histogram) measurements. The shadowed areas denote the uncertainty on the fitted parameters.

The agreement shown in Fig. 8 between the results of the data analyses both in isothermal and in CRR conditions suggests that the different thermal treatments employed in the TD measurements do not appreciably alter the effusion process and that in first approximation the He desorption proceeds always through quasi equilibrium configurations, at least after a thermal treatment corresponding to the rise time.

V. DISCUSSION

The experimental results suggest the presence of interaction processes among He and Si crystal or Si defects with distributed interaction energies. Moreover, as evidenced by the isothermal results, the processes responsible for the initial increase and for the subsequent decrease of the desorption rate curves have comparable activation energies and need to be interpreted with a comprehensive model. In such a model other results reported in the literature should also be included and in particular the formation of voids. The presence of He must play a fundamental role in the process, since the radiation damage itself does not necessarily evolve towards the formation of the bubbles. Moreover, the appearance of the bubbles results correlated to the He local concentration[4] rather than to the total ion dose or the implantation energy. Finally, the theoretical predictions that He is not trapped at single vacancies and that it is able to form interstitial clusters in a perfect Si crystal suggest that it is reasonable to propose a model for void production where He is supposedly the only agent.

A semiquantitative model which enables us to rationalize the results can be constructed referring to the large quantity

of data available on He in metals. If we assume that He in Si has a similar behavior with tendency towards clustering, the binding energy of the $(n+1)$th He atom to an existing cluster of n He atoms increases with n up to the condition of maximum packing[23] that, for Si lattice, is presumably around the minimum allowed by the structure, i.e., $n \approx 4$. By increasing the He local concentration, the cluster can grow and reach a critical dimension that allows the formation of a number of adjacent Si vacancies capable to accommodate all the existing He atoms. The energy for the production of the needed Frenkel pairs comes from the exothermic transfer of the He atoms from solid solution to the gas phase into the created void. A rough estimate of the critical cluster dimension can be performed assuming the blister composed of four vacancies and the Frenkel pair average creation energy of 5 eV: the number of required He atoms is at least 30. From this guess, the gas pressure into the blister should be of the order of 10^9 Pa. Such a pressure, especially for the smaller blisters, can facilitate the He reemission allowing He effusion at relatively low temperatures. In terms of energy, He-He hard-core repulsion effects, He interaction with the blister walls and, presumably, quantum effects due to He confinement are factors that contribute to lower the He solution enthalpy from these sinks. Such effect vanishes with decreasing gas pressure and with the evolution of the blisters towards the stable configuration typical of the bubble in Si. In this sense, an operative definition of bubble precursor can be that cavity where there are relevant He atoms mutual interactions as well as the interactions with the walls, characterized by a He solution enthalpy lower than ΔH_s.

The discussion will proceed considering the presence of such He-filled nanoblisters even in the as-implanted sample. At the He dose here employed, the peak concentration is close to the critical value for bubble formation and He-He interactions are highly probable. The most probable state of He in the as-implanted sample is in the gas phase into small vacancy clusters. It is not excluded, however, that impurities such as O, C, or dopants, normally present in various concentrations in commercial Si wafers, can act as nanoblister nucleation sites or that the vacancies produced during the implant can contribute to the blister growth. Besides the He atoms contained in the nanoblisters, some small He interstitial clusters as well as isolated He atoms can still be present, especially in the boundaries of the defective region of the implantation peak.

From the agreement between the results from isothermal and CRR measurements, we will refer for simplicity only to the first ones. The CRR measurements will be employed to qualitatively deduce the influence of the He dose. In the first stages of the isothermal treatments, the system, created by the implantation process far from thermodynamic equilibrium, evolves towards a more equilibrium situation through those processes allowed at the temperature of the thermal treatment. The rise time can be regarded as the time required by the system to reach a quasiequilibrium state where all the He atoms are trapped into nanoblisters at a pressure roughly homogeneous within the defective region. The characteristic time for such initial process can be evaluated as the time spent by the He atoms to diffuse throughout the defective region (the defect-free region does not limit the effusion kinetics):

$$t_r = \Delta X^2 / D^*, \tag{8}$$

where ΔX is the thickness of the region where the trap are present and D^* is the effective diffusion coefficient given by

$$D^* = D \frac{\overline{\tau}}{\tau^* + \overline{\tau}} \approx D \frac{\overline{\tau}}{\tau^*}, \quad \tau^* \gg \overline{\tau}, \tag{9}$$

where $\overline{\tau}$ is the average nonthermally activated time between two serial collisions with the traps and τ^* the average trapping time. The activation energy evaluated on t_r can be interpreted as the sum of the He migration energy in Si (due to D) and the He enthalpy of solution from the nanoblisters (due to τ^*): $E_r = \Delta H_s^* + E_m$. In our case ΔH_s^* results in $E_r - E_m \approx 0.4$ eV. This value, much lower than the solution energy ΔH_s, indicates that we are in the presence of those traps we have named bubble precursors.

The decreasing part of $r(t)$ occurs in a quasisteady state where the desorption can be considered the outdiffusion of an activated concentration. The effective activation energy of this process is the sum of the solution energy from the traps and the energy barrier E_{outdiff} for outdiffusion that for He in Si is expected to be very similar to, or at most slightly lower than, the migration energy: $E = \Delta H_s^* + E_{\text{outdiff}}$. This analysis explains the similarity between the experimental values of $E_r = 1.3$ eV and $E = E_{\min} = 1.17$ eV since they are obtained in similar conditions of desorbed He quantities. The energy heterogeneity exhibited by the desorption process can be attributed to the variations of the contribution of ΔH_s^* in the effective activation energy that assumes its lowest value at the beginning of the process when the He pressure into the nanoblister is maximum then increases and, in principle, can reach the unperturbed value $\Delta H_s = 0.9$ eV, typical of He in relatively large voids. Such interpretation of the experimental results is compatible with the concept of induced heterogeneity since the effective activation energy measured at time t is related to the pressure inside the nanoblisters that depends on the He concentration still present into the sample. Fixed heterogeneity is also present, for the simultaneous presence of various traps differently decorated, but its effect on the desorption kinetics is minimized by the He traps homogenization occurring during the early stages of the thermal treatment.

The evolution of the system with He implantation doses can be qualitatively deduced from the CRR spectra of Fig. 2. Below the critical concentration for bubble formation (doses of 1.4×10^{15} and 5×10^{15} cm^{-2}) only the peak arising from He bonded to the precursors is observed. As the dose is increased this He desorbs at higher temperatures, indicating the presence of stronger traps (larger voids) and the peak typical of the bubbles appears at 700 °C. Bubbles are presumably formed by coalescence of smaller voids during the thermal treatment.

VI. CONCLUSIONS

In conclusion, we have studied the defects formed by He ion implantation in Si near the critical conditions for bubble formation. The technique employed, thermal desorption spectrometry, allows information to be obtained about the interactions of the He atoms with these defects, in terms of their dissociation energy. The data analysis of the He re-

leased in the temperature range 200–500 °C has revealed the presence of heterogeneous traps characterized by an effective activation energy spread of about 0.2 eV starting from a minimum effusion energy of about 1.1 eV.

To explain our results, a semiquantitative model, based on the present knowledge about the Si:He system, has been proposed. This model accounts for He-filled nanoblister formation through interstitial He clustering and precipitation. These sinks have been called the precursors of the bubbles. The model, in agreement with our results, suggests that, due to He-He and He-wall interactions into the nanoblisters, the solution energy from these traps varies during the thermal treatment and, especially at the beginning of the thermal emission process, it can result in decidedly lower He solution energy evaluated by permeation experiments.

ACKNOWLEDGMENTS

This work was partially supported by M.U.R.S.T. and has been performed in the framework of the collaboration between the Laboratorio Materiali e Dispositivi per la Microelettronica of the Istituto Nazionale per la Fisica della Materia and SGS Thomson Microelectronics.

APPENDIX: DERIVATION OF THE PARAMETRIC EQUATION OF THE THERMAL DESORPTION RATE IN PRESENCE OF ENERGY HETEROGENEITY

All the multiplication constants will be omitted and the normalization condition will be applied to the result.

Substituting Eqs. (5) and (6) into Eq. (4), we obtain the expression of the heterogeneous isotherm in the case of the assumed energy distribution function:

$$C_h(t)=\int_{E_{\min}}^{E_{\max}}\exp\left(-\frac{t}{\tau_0\,\exp(E/k_BT)}\right)\exp\left(-\frac{E}{\Delta}\right)dE. \tag{A1}$$

The need of knowing the value of τ_0 is eliminated with the integration variable substitution $E\rightarrow k_BT\,\ln(\tau/\tau_0)$ leading to the equation:

$$C_h(t)=\int_{\tau_{\min}}^{\tau_{\max}}\exp\left(-\frac{t}{\tau}\right)\tau^{-(1+s)}d\tau, \tag{A2}$$

where $\tau_{\min}=\tau_0\exp(E_{\min}/k_BT)$, $\tau_{\max}=\tau_0\exp(E_{\max}/k_BT)$, and $s=k_BT/\Delta$.

A more simple form can be obtained performing the substitution $t/\tau\rightarrow x$ leading to

$$\begin{aligned}C_h(t)&=-t^{-s}\int_{t/\tau_{\min}}^{t/\tau_{\max}}x^{s-1}\exp(-x)dx\\&=-t^{-s}\Gamma\left(s,\frac{t}{\tau_{\min}},\frac{t}{\tau_{\max}}\right),\end{aligned} \tag{A3}$$

where the generalized incomplete gamma function appears.

The desorption rate is obtained by time differentiation of Eq. (A3):

$$r_h(t)=\frac{d}{dt}\left[t^{-s}\Gamma\left(s,\frac{t}{\tau_{\min}},\frac{t}{\tau_{\max}}\right)\right]=t^{-(1+s)}\left\{\left[\tau_{\max}^{-s}\exp\left(-\frac{t}{\tau_{\max}}\right)-\tau_{\min}^{-s}\exp\left(-\frac{t}{\tau_{\min}}\right)\right]t^{s}-s\Gamma\left(s,\frac{t}{\tau_{\min}},\frac{t}{\tau_{\max}}\right)\right\}. \tag{A4}$$

Finally, the normalization condition is satisfied by imposing $\int_0^{+\infty}r_h(t)dt=C_0$.

[1] C. C. Griffioen, J. H. Evans, P. C. de Jong, and A. van Veen, Nucl. Instrum. Methods Phys. Res. Sec. B **27**, 417 (1987).
[2] J. H. Evans, A. van Veen, and C. C. Griffioen, Nucl. Instrum. Methods Phys. Res. Sec. B **28**, 360 (1987).
[3] V. Raineri, A. Battaglia, and E. Rimini, Nucl. Instrum. Methods Phys. Res. Sec. B **96**, 249 (1995).
[4] V. Raineri, P. G. Fallica, G. Percolla, A. Battaglia, M. Barbagallo, and S. U. Campisano, J. Appl. Phys. **78**, 3727 (1995).
[5] D. M. Follstaedt, Appl. Phys. Lett. **62**, 1116 (1993).
[6] D. J. Eaglesham, A. E. White, L. C. Feldman, N. Moriya, and D. C. Jacobson, Phys. Rev. Lett. **70**, 1643 (1993).
[7] D. M. Follstaedt, S. M. Myers, and H. J. Stein, in *Beam-Solid Interactions: Fundamentals and Applications*, edited by M. A. Nastasi *et al.*, MRS Symposia Proceedings No. 279 (Materials Research Society, Pittsburgh, 1993), p. 105.
[8] C. H. Seager, S. M. Myers, R. A. Anderson, W. L. Warren, and D. M. Follstaedt, Phys. Rev. B **50**, 2458 (1994).
[9] S. M. Myers, D. M. Follstaedt, and D. M. Bishop, in *Materials Synthesis and Processing Using Ion Beams*, edited by R. J. Culbertson *et al.*, MRS Symposia Proceedings No. 316, (Materials Research Society, Pittsburgh, 1994), p. 33.
[10] M. H. F. Overwijk, J. Politiek, R. C. M. de Kruif, and P. C. Zalm, Nucl. Instrum. Methods Phys. Res. Sec. B **96**, 257 (1995).
[11] V. Raineri and S. U. Campisano, Appl. Phys. Lett. **66**, 3654 (1995).
[12] V. Raineri and S. U. Campisano, Appl. Phys. Lett. **69**, 1783 (1996).
[13] M. van Wieringen and N. Warmoltz, Physica (Utrecht) **22**, 849 (1956).
[14] P. Jung, Nucl. Instrum. Methods Phys. Res. Sec. B **91**, 362 (1994).
[15] M. Alatalo, M. J. Puska, and R. M. Nieminen, Phys. Rev. B **46**, 12 806 (1992).
[16] P. A. Redhead, Vacuum **12**, 203 (1962).
[17] G. Carter, Vacuum **12**, 245 (1962).
[18] C. Aharnoi and F. C. Tompkins, Adv. Catal. **21**, 1 (1970).
[19] G. F. Cerofolini and N. Re, J. Colloid Interface Sci. **174**, 428 (1995).
[20] J. F. Ziegler, J. P. Biersack, and U. Littmark, *The Stopping and Range of Ions in Solids* (Pergamon, New York, 1985).
[21] A. van Veen, A. H. Reader, D. J. Gravesteijn, and A. A. van Gorkum, Thin Solid Films **241**, 206 (1993).
[22] C. M. Chan, R. Aris, and W. H. Weinberg, Appl. Surf. Sci. **1**, 360 (1978).
[23] W. D. Wilson, C. L. Bisson, and M. I. Baskes, Phys. Rev. B **24**, 5616 (1981).